ACS MATERIALS LETTERS

www.acsmaterialsletters.org

LETTER

Divergent Electrically Conductive Pathways in Yttrium-Based 2- and 3-Dimensional Metal–Organic Frameworks

Connor Welty,[†] Eoghan L. Gormley,[†] Julius J. Oppenheim, Mircea Dincă, Christopher H. Hendon,* and Nicholas P. Stadie*

Cite This: *ACS Materials Lett.* 2024, 6, 3909–3914

Read Online

ACCESS | Metrics & More | Article Recommendations | Supporting Information

ABSTRACT: **Despite most porous framework solids exhibiting insulating character, some are known to conduct electrical charge. The peak performing conductive metal–organic frameworks are composed of redox-active hexasubstituted triphenylene linkers, but the impact of redox activity on material conductivity remains enigmatic because of limited availability of direct structure–function relationships. Here, we report a hexagonal yttrium-based conductive porous scaffold, comprising hexahydroxytriphenylene connected by Y-chains (YHOTP). In comparison to its known porous cubic counterpart (Y_6HOTP_2), this material features a 1000-fold increase in peak conductivity in polycrystalline samples ($\sim 10^{-1}$ S cm^{-1}). Furthermore, through a comparison of their electronic structures, we rationalize the origin of this difference and highlight the role of charge carrier concentration in dictating bulk electrical conductivity. Together, this work provides a design principle for the development of next-generation conductive porous frameworks.**

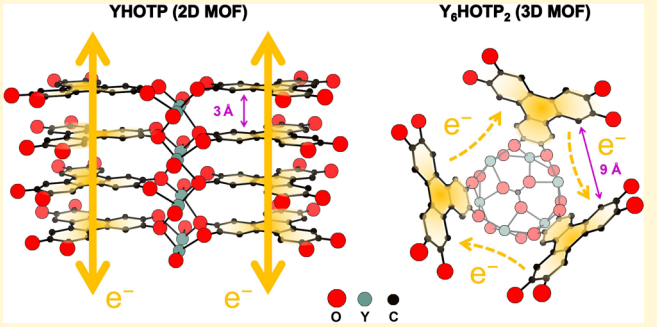

Most metal–organic frameworks (MOFs) are electrical insulators due to energetic mismatch between the metal clusters and the ligands that support them.[1−3] MOFs that do conduct electricity feature conductive pathways that permit charge mobility either through space (through π-stacking or other secondary bonding)[4] or through bond (through dative, ionic, or covalent bonds),[5] and are potentially useful as active materials in electrocatalysis[6−8] and in electrochemical energy storage devices.[9−13] To date, the highest performing conductive MOFs feature conductivity values exceeding 100 S cm^{-1} and are through-space conductors. Effort has been invested in understanding how the spatial orientation of the MOF components dictates the crystal conductivity, however very few structure–function relationships have been revealed. A comparison of compositionally similar frameworks with dissimilar geometries is required to elucidate basic principles that underpin electrical conduction in molecular materials.

Since electrical conductivity is primarily dictated by the number and mobility of charge carriers, interest has been focused on methods to affect band curvature and the free carrier concentration in the materials. Toward the latter, two strategies have been developed; either through electrochemical doping[14] or through narrowing of the electronic band gap via ligand functionalization.[15] With the exception of mixed-valent Fe-based frameworks, the most conductive MOFs are composed of hexasubstituted triphenylenes (e.g., hexahydroxytriphenylene, HHTP, which is referred to as HOTP once incorporated into the framework)[16] and their synthesis does not afford an obvious route to introduce functionalization beyond the ligating atoms themselves.[17−19] Instead, those linkers are known to oxidize during self-assembly, introducing charge carriers through redox events. Once assembled, the charge carriers are thought to traverse the closely spaced π-stacked layers, leading to anisotropic through-space conduction.[20,21]

When paired with first row transition metals (e.g., Co, Ni, Cu),[22−24] the resultant 2D-connected layered materials exhibit among the highest known electrical conductivity of any MOFs to date. Stacking faults may disrupt the π-overlap between

Received: May 26, 2024
Revised: July 21, 2024
Accepted: July 22, 2024
Published: July 26, 2024

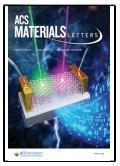

https://doi.org/10.1021/acsmaterialslett.4c01102
ACS Materials Lett. 2024, 6, 3909–3914

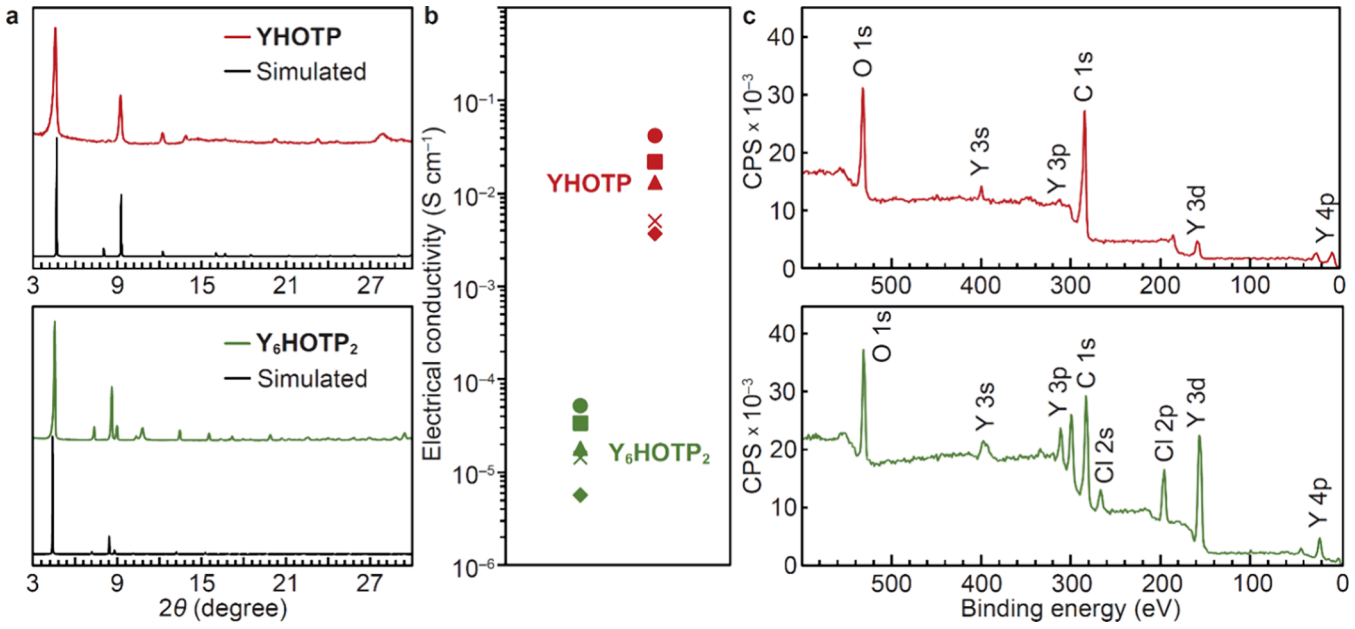

Figure 1. Materials characterization comparison of YHOTP and Y_6HOTP_2. (a) Powder XRD patterns revealing that the microcrystalline sample is highly crystalline. (b) Pressed pellet conductivities of five different batches of each MOF. (c) XPS shows the presence of Cl in the Y_6HOTP_2, and differences in the C 1s binding energy, attributed to differences in linker oxidation state.

layers, and subsequently result in variable and reduced conductivity. Larger metal cations (e.g., La, Ho, Nd, Yb) have been shown to reduce stacking faults and form large crystals.[25] In those cases, the metals sit between the organic sheets and, like the other 2D-conductive MOFs, those formed from *f*-block elements are known to be in-plane insulators, and out-of-plane metals. Meanwhile, some of the same metal ions can be used to form a 3D-connected cubic framework, with reported structures made from La, Eu, and Y.[26] Thus, the formation of iso-compositional frameworks with dissimilar connectivity, but high degrees of covalency remain key targets in MOF syntheses.

Noting that Y^{3+} supports a larger coordination sphere than its kainosymmetric azimuthal analogue (Sc^{3+}), we surmised that Y could be used to form the tightly spaced layered structure of MHOTP. In doing so, Y would be the only *d*-block element capable of reliably forming both the hexagonal and cubic structures, permitting a controlled analysis of the properties that drive electrical conduction in this class of materials. Here, we report the synthesis of YHOTP, and through comparison with its known cubic 3D counterpart, Y_6HOTP_2, we show that the spatial orientation of the linkers dictates the conductive pathways due to divergent linker behavior. The 2D material exhibits strong intermolecular electron and hole charge transfer coupling, while the 3D structure hosts high charge carrier concentrations.

To target the layered hexagonal 2D structure, YHOTP was obtained by mixing $Y(NO_3)_3{\cdot}6H_2O$ with HHTP in a mole ratio of 10:1 in a mixture of water, *N,N′*-dimethylimidazolidinone (DMI), and sodium acetate (NaOAc). The reaction mixture was held at 80 °C for 16 h in air, then washed and dried to obtain $(YOH)_{1-x}HOTP(H_2O)_n$ (x = 0 to 0.2; referred to as **YHOTP**). Y-vacancies are accounted for with positive values of x. To obtain the cubic 3D structure, YCl_3 was used in a metal:linker mole ratio of 80:1. To promote crystallization and disincentivize oxidation, the mixture was heated to 135 °C for 72 h in a nitrogen-filled glovebox in a similar solvent mixture. The resultant material, $Y_6(HOTP)_2(CO_3)Cl_6$ (**Y_6HOTP_2**) was obtained. We surmised that the carbonate was formed during self-assembly through solvent decomposition, and trace nitrogen in the elemental analysis likely corresponds to trapped solvent within the pores. Both products' chemical compositions were determined by a combination of single-crystal X-ray diffraction (XRD), X-ray photoelectron spectroscopy (XPS), and elemental analysis (**Tables S1−S6**). Microcrystalline samples of each product were found to have the same crystallographic structure as that of the bulk single crystals of each MOF (Figure 1a).

Following the reported procedure for measuring electrical conductivity on polycrystalline samples, pressed pellet conductivities were determined in pentaplicate, using a two-point probe device detailed in the Experimental Methods. The hexagonal 2D framework, **YHOTP**, consistently exhibited at least 1000× higher conductivity than its cubic 3D counterpart, with a peak conductivity of $\sim 3 \times 10^{-1}$ S cm^{-1} (Figure 1b). A similar conclusion is predicted through a comparison of the computed electronic band structures (Figure 2). However, despite the cubic material possessing an insulating ground state electronic structure,[8] the material has surprisingly high peak conductivities of $\sim 10^{-4}$ S cm^{-1}, which is as much as 9 orders of magnitude greater than MOFs with comparable band gaps.[5] Thus, we surmised that another effect may be dictating the electrical conduction in these frameworks.

One explanation for this divergence could be a difference in charge carrier concentration. Since we are unable to grow single crystals large enough to perform a Hall measurement, we instead deduce the concentration from theory. By comparing the curvature of the bands in the direction with the lightest holes and electrons (Γ−A for **YHOTP**, Γ−X for **Y_6HOTP_2**), the electronic band structure calculations reveal approximately 2 orders of magnitude difference in effective mass of the charge carriers, with the heavier carrier belonging to **Y_6HOTP_2**. Since conductivity is proportional to the charge carrier concentration and mobility, and the differences in mobility are of the same

https://doi.org/10.1021/acsmaterialslett.4c01102
ACS Materials Lett. 2024, 6, 3909−3914

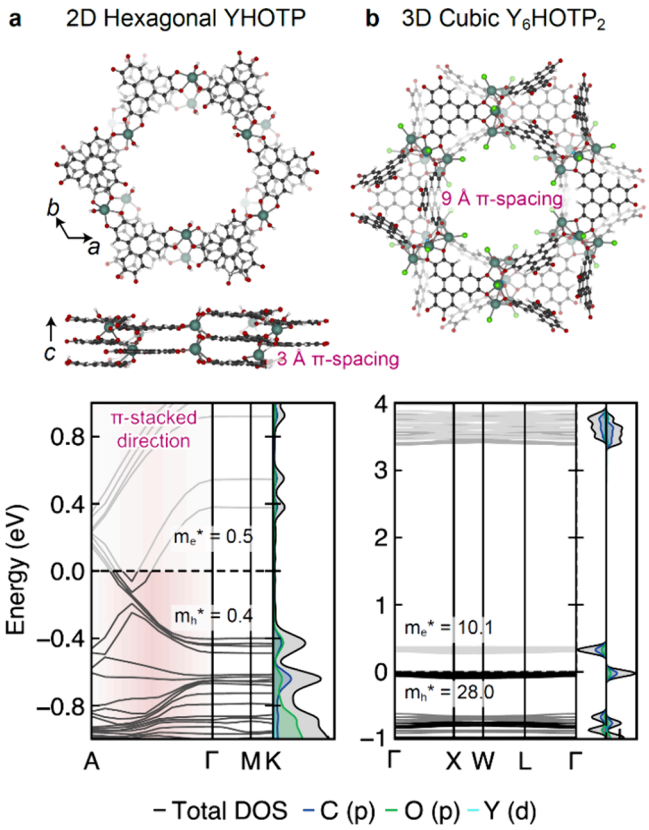

Figure 2. (a) The hexagonal (YHOTP) and (b) cubic (Y_6HOTP_2) crystal structures and corresponding electronic band structures. The former has pathways of through-space π-interactions, while the latter features isolated chemical motifs. The proximity of π-clouds in YHOTP is reflected in its electronic band structure, where it is predicted to be an out-of-plane metal and in-plane narrow gap insulator. Y_6HOTP_2 is predicted to be a narrow gap insulator due to limited spatial overlap throughout the crystal, with band edge densities localized on the ligand. Charge carrier effective masses are labeled. C, O, Cl, H, and Y are depicted in black, red, green, white, and sage, respectively.

order of magnitude as the pressed-pellet conductivity, the corresponding carrier concentration must not vary by more than 1 order of magnitude.

Considering the composition differences, and that the XPS data presented in Figure 1c indicate that Y exists in the 3+ oxidation state, the differences in conductivity are driven by a combination of dissimilar linker oxidation state and intermolecular orientation. Since the 2D structure only forms in the presence of air, it is understood that the linker oxidizes during self-assembly. With complementary deprotonation, the hexagonal layered material hosts linkers with nominal 3− charge. This charge should result in a single unpaired electron per linker but solid-state EPR reveals **YHOTP** has substantially less radical character than the cubic analogue (Figure S1), which has been previously attributed to linker vacancies rather than native ligand-centered unpaired electrons.[25] Thus, we surmised that the linkers rather exist as a delocalized 2− and 4− pair, an electronic configuration common in the 2D conductive family of frameworks.[20]

Conversely, **Y_6HOTP_2** forms under a nitrogen atmosphere and, hence, should be less oxidized. In its case, the linkers exhibit a formal 5− charge. In this charge state, the linkers are nominally more aromatic than their oxidized counterparts and should host unpaired electrons. EPR revealed a ligand-centered radical associated with a single unpaired electron per linker (Figure S1). The difference concentration in mobile charge carriers cannot vary by more than one electron per linker, supporting our offering that the difference in charge carrier concentration will never exceed 1 order of magnitude. This may be the origin of elevated conductivity in **Y_6HOTP_2** compared to other similarly flat-banded materials — the linker is likely installing large numbers of charge carriers.

Both **YHOTP** and **Y_6HOTP_2** are through-space conductors but have different ligand geometries. This is generally interesting because intermolecular distances usually increase with increasing porosity, and these frameworks serve as a platform to understand how orientation impacts through-space conduction, and whether having spatially separated ligands can permit charge transfer between them. To do so, we turn to Marcus theory to assess the charge transfer coupling between neighboring ligands. We created two models from the bulk crystals, each featuring a pair of linkers with their geometry remaining fixed, as imposed by the geometry obtained for the crystal.[27] The linkers were then protonated to create a charge-neutral system (Figure 3). The electron and hole couplings for

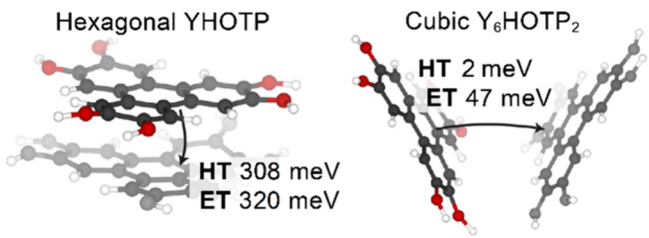

Figure 3. A comparison of the hexagonal (YHOTP) and cubic (Y_6HOTP_2) ligand charge transfer interactions. The electron coupling (ET) is consistently larger than the hole coupling (HT) driven by the propensity for the ligands to rearomatize. C, O, and H are depicted in black, red, and white, respectively.

each cluster were calculated using CATNIP.[28] For comparison, the cluster's molecular orbitals were also computed using the ZINDO method (Figure S4), and the electron and hole couplings were then extracted using the Molecular Orbital Overlap (MOO) method.[29] For the cubic system, the hole transfer coupling was found to be 2 meV, while the electron coupling was 47 meV. Both of these values are extremely weak. The hexagonal crystal featured coupling energies of 320 and 308 meV for the electron and hole, respectively. These values are relatively large and are comparable to other organic charge transfer aggregates.[30,31] Together we surmise that for the hexagonal system, the mobility of the charge carriers is high reflected in the band structure and also in the hole and electron coulping energies. Conversely, the cubic system features weak couplings, and highly localized electronic bands.

By further computing the reorganization energies for both the electron and hole transfer to the protonated ligand, the rate of charge transfer can also be computed. Since the linkers are the same for both the cubic and hexagonal phase, the reorganization energies should be roughly the same for both systems: 587 meV for electron reorganization and 491 meV for hole reorganization. Applying Marcus theory, the Arrhenius rates of charge transfer for the hexagonal system are then 7.5×10^{12} s^{-1} and 1.9×10^{13} s^{-1} for electron and hole transfer, respectively. The cubic material exhibits rates 2−4 orders of magnitude slower: 1.6×10^{11} s^{-1} and 6.6×10^{8} s^{-1} for electron

https://doi.org/10.1021/acsmaterialslett.4c01102
ACS Materials Lett. 2024, 6, 3909−3914

and hole transfer, respectively. These calculations suggest that differences in conductivity are further dictated by differences in charge transfer rates, associated with differences in geometry.

Thus, through the isolation of a Y-based hexagonal layered conductor, **YHOTP**, and by comparison to its cubic counterpart, $\mathbf{Y_6HOTP_2}$, we can make several conclusions. Given that the coupling energies in the latter are extremely weak, but its charge carrier effective masses are comparable to other flat-band insulators, the reason for its surprisingly high conductivity ($\sim 10^{-4}$ S cm^{-1}) is likely due to the differences in linker oxidation state, which we believe is directly influencing the charge carrier concentration in the MOF. Further, given that the linker is more aromatic in the 3D framework — a property that is typically inversely proportional to conductivity[32] — this strongly indicates that linker redox is a critical and primary deciding factor dictating electrical charge conduction in MOFs, and highlights that the interplay between linker redox potential and orientation dictates bulk conductivity. Looking forward, these findings help rationalize why the HOTP-based materials are the best conductors in their class and should instruct future efforts to diversify ligand design.

EXPERIMENTAL SECTION

Synthesis of YHOTP and $\mathbf{Y_6HOTP_2}$. Prior to synthesis, HHTP was dissolved in DMI and recrystallized from hot H_2O to remove impurities. For the synthesis of **YHOTP**, 0.63 mmol of $Y(NO_3)_3{\cdot}6H_2O$ was dissolved in 3 mL of deionized H_2O in a 20 mL scintillation vial in air. 0.063 mmol of HHTP was dissolved in 0.8 mL of DMI and the two solutions were combined. A solution of 0.189 mmol of NaOAc dissolved in 0.6 mL of deionized H_2O was added to the mixture. The mixture was transferred to a 15 mL pressure tube containing sanded glass slides and heated at 80 °C for 16 h. For the synthesis of $\mathbf{Y_6HOTP_2}$, 4.8 mmol of $YCl_3{\cdot}6H_2O$ was dissolved in 3 mL of deionized H_2O and added to a solution of 0.06 mmol of HHTP dissolved in 0.8 mL of DMI in a N_2-filled glovebox. 0.18 mmol of NaOAc dissolved in 0.6 mL of deionized H_2O was added to the mixture and then the solution was filtered into a 15 mL pressure tube containing sanded glass slides using a 0.2 μm PTFE filter. The reaction was heated at 135 °C for 72 h and then brought back into the N_2-filled glovebox. The mother liquor was decanted and the resulting powder was washed 3× with deoxygenated DI water and 3× with deoxygenated methanol. Both samples were activated by drying under vacuum at 90 °C for 1 h.

Electrical Conductivity Measurements. Two-point probe measurements were made on activated pressed pellets using a custom apparatus previously described.[33] 2−3 mg of powder was loaded into a glass tube and compressed by copper rods that also served as leads. The apparatus was compressed using a hydraulic press while dual linear I−V curves were obtained using a Keithley 2450 source meter. The pellets were further compressed between I−V measurements until the change in resistance was low (Figure S2). The conductivity measurements were made in pentaplicate.

Materials Characterization. Powder XRD measurements were performed using a Bruker D8 Advance diffractometer with Cu K$\alpha_{1,2}$ radiation (λ = 1.54 Å) in reflection geometry. XPS measurements were performed using a Physical Electronics VersaProbe II photoelectron spectrometer with monochromatized Al Kα radiation (E = 1486.6 eV). Binding energy was calibrated by shifting the main C 1s peak to 284.8 eV. EPR was performed using a Magnettech ESR5000 spectrometer with a microwave power of 20 mW and an amplitude of 0.3 G.

Computational Methods. Density functional theory (DFT) calculations were performed using the Vienna *ab initio* Simulation Package (VASP).[34] All structures were optimized using the PBEsol functional with a plane wave energy cutoff of 500 eV, and an ionic convergence criterion of −0.005 eV. Bulk **YHOTP** was optimized using a 2 × 2 × 5 k-mesh to sample the first Brillouin zone, and all structures involving $\mathbf{Y_6HOTP_2}$ used a Γ-only k-mesh due to the size of the unit cell and the resulting computational cost of the calculation. $\mathbf{Y_6HOTP_2}$ is charge-balanced by disorder guest molecules in the pores. Here, we achieved charge balance by adding one Cl per Y, capping the open metal sites in the metal clusters. The electron count was adjusted by the removal of 4 electrons, achieving charge neutrality. This strategy significantly reduced the net charge of the structure in the calculations, aligned with the experimental number of charges on each linker from EPR, and is justified due to the presence of Cl in the elemental analysis. We also tested an alternate charge balancing method, by removing the chlorides and subtracting 20 electrons (2.5 per linker) from the system. The former strategy yielded a plausible structure that was then used for the electronic band structure calculation. The HSEsol hybrid functional[35] was used to compute the band structures. Charge transfer calculations were performed on clusters of HOTP ligands extracted from the geometrically equilibrated crystal structures and protonated to achieve charge neutrality. Initial calculations were performed using the ZINDO method[29] (Figure S4), as implemented in Gaussian09,[36] and yielded similar coupling energies as computed by ab initio methods (using CATNIP[28] with the B3LYP functional and 6-31G basis set, as shown in Figure 3). Coupling energies were calculated from the resulting molecular orbitals using the MOO method.[29]

ASSOCIATED CONTENT

Supporting Information

The Supporting Information is available free of charge at https://pubs.acs.org/doi/10.1021/acsmaterialslett.4c01102.

Further synthetic and experimental details, supplemental calculations, physical characterization, and supporting tables and figures (PDF)

AUTHOR INFORMATION

Corresponding Authors

Christopher H. Hendon − *Department of Chemistry and Biochemistry, University of Oregon, Eugene, Oregon 97403, United States*; orcid.org/0000-0002-7132-768X; Email: chendon@uoregon.edu

Nicholas P. Stadie − *Department of Chemistry and Biochemistry, Montana State University, Bozeman, Montana 59717, United States*; orcid.org/0000-0002-1139-7846; Email: nstadie@montana.edu

Authors

Connor Welty − *Department of Chemistry and Biochemistry, Montana State University, Bozeman, Montana 59717, United States*

Eoghan L. Gormley − *Department of Chemistry and Biochemistry, University of Oregon, Eugene, Oregon 97403, United States*

https://doi.org/10.1021/acsmaterialslett.4c01102
ACS Materials Lett. 2024, 6, 3909−3914

Julius J. Oppenheim − *Department of Chemistry, Massachusetts Institute of Technology, Cambridge, Massachusetts 02139, United States;* orcid.org/0000-0002-5988-0677

Mircea Dincă − *Department of Chemistry, Massachusetts Institute of Technology, Cambridge, Massachusetts 02139, United States;* orcid.org/0000-0002-1262-1264

Complete contact information is available at: https://pubs.acs.org/10.1021/acsmaterialslett.4c01102

Author Contributions

†C.W. and E.L.G. contributed equally. The manuscript was written through contributions of all authors. CRediT: **Connor Welty** data curation, formal analysis, investigation, methodology, writing-original draft; **Eoghan Gormley** data curation, formal analysis, investigation, software, writing-original draft; **Julius J. Oppenheim** data curation, formal analysis, investigation, writing-review & editing; **Mircea Dinca** conceptualization, project administration, supervision, writing-review & editing; **Christopher H. Hendon** conceptualization, data curation, formal analysis, funding acquisition, investigation, methodology, software, supervision, validation, visualization, writing-original draft, writing-review & editing; **Nicholas P. Stadie** conceptualization, data curation, formal analysis, funding acquisition, investigation, methodology, project administration, supervision, validation, writing-original draft, writing-review & editing.

Notes

The authors declare no competing financial interest.

■ ACKNOWLEDGMENTS

We thank Grigorii Skorupskii for synthetic insights, Andrei Iliescu for performing the XPS experiments, and Isaac Sanchez for assistance with the EPR experiments. C.W. and N.P.S. are grateful for funding provided by the National Science Foundation Office of Integrated Activities (award OIA-2034110). Computational aspects of this paper are supported by the National Science Foundation through the Division of Materials Research (award DMR-1956403) and the Camille and Henry Dreyfus Foundation. Work in the Dincă lab was supported by the Department of Energy (award DE-SC0023288). This work was performed using Expanse at the San Diego Supercomputing Center (SDSC) through allocation CHE-160003 and CHE-230070 from the Advanced Cyberinfrastructure Coordination Ecosystem: Services & Support (ACCESS) program, which is supported by the National Science Foundation (grants 2138259, 2138286, 2138307, 2137603, and 2138296).

■ REFERENCES

(1) Li, C.; Zhang, L.; Chen, J.; Li, X.; Sun, J.; Zhu, J.; Wang, X.; Fu, Y. Recent Development and Applications of Electrical Conductive MOFs. *Nanoscale* **2021**, *13*, 485−509.

(2) Hendon, C. H.; Rieth, A. J.; Korzynski, M. D.; Dincă, M. Grand Challenges and Future Opportunities for Metal-Organic Frameworks. *ACS Cent. Sci.* **2017**, *3*, 554−563.

(3) Syzgantseva, M. A.; Stepanov, N. F.; Syzgantseva, O. A. Band Alignment as the Method for Modifying Electronic Structure of Metal-Organic Frameworks. *ACS Appl. Mater. Interfaces* **2020**, *12*, 17611−17619.

(4) Hua, C.; Doheny, P. W.; Ding, B.; Chan, B.; Yu, M.; Kepert, C. J.; D'Alessandro, D. M. Through-Space Intervalence Charge Transfer as a Mechanism for Charge Delocalization in Metal-Organic Frameworks. *J. Am. Chem. Soc.* **2018**, *140*, 6622−6630.

(5) Xie, L. S.; Skorupskii, G.; Dincă, M. Electrically Conductive Metal-Organic Frameworks. *Chem. Rev.* **2020**, *120*, 8536−8580.

(6) Wang, H. F.; Chen, L.; Pang, H.; Kaskel, S.; Xu, Q. MOF-Derived Electrocatalysts for Oxygen Reduction, Oxygen Evolution and Hydrogen Evolution Reactions. *Chem. Soc. Rev.* **2020**, *49*, 1414−1448.

(7) Jin, S. How to Effectively Utilize MOFs for Electrocatalysis. *ACS Energy Lett.* **2019**, *4*, 1443−1445.

(8) Liu, J.; Zhu, D.; Guo, C.; Vasileff, A.; Qiao, S. Z. Design Strategies toward Advanced MOF-Derived Electrocatalysts for Energy-Conversion Reactions. *Adv. Energy Mater.* **2017**, *7*, 1700518.

(9) Zhang, H.; Liu, X.; Wu, Y.; Guan, C.; Cheetham, A. K.; Wang, J. MOF-Derived Nanohybrids for Electrocatalysis and Energy Storage: Current Status and Perspectives. *Chem. Commun.* **2018**, *54*, 5268−5288.

(10) Tahir, M. A.; Arshad, N.; Akram, M. Recent Advances in Metal Organic Framework (MOF) as Electrode Material for Super Capacitor: A Mini Review. *J. of Energy Storage* **2022**, *47*, 103530.

(11) Sheberla, D.; Bachman, J. C.; Elias, J. S.; Sun, C. J.; Shao-Horn, Y.; Dincă, M. Conductive MOF Electrodes for Stable Supercapacitors with High Areal Capacitance. *Nat. Mater.* **2017**, *16* (2), 220−224.

(12) Maiti, S.; Pramanik, A.; Dhawa, T.; Sreemany, M.; Mahanty, S. Bi-Metal Organic Framework Derived Nickel Manganese Oxide Spinel for Lithium-Ion Battery Anode. *Mater. Sci. & Eng. B* **2018**, *229*, 27−36.

(13) Song, W.; Teng, X.; Liu, Y.; Wang, J.; Niu, Y.; He, X.; Zhang, C.; Chen, Z. Rational Construction of Self-Supported Triangle-Like MOF-Derived Hollow (Ni,Co)Se_2 Arrays for Electrocatalysis and Supercapacitors. *Nanoscale* **2019**, *11*, 6401−6409.

(14) Park, J. G.; Aubrey, M. L.; Oktawiec, J.; Chakarawet, K.; Darago, L. E.; Grandjean, F.; Long, G. J.; Long, J. R. Charge Delocalization and Bulk Electronic Conductivity in the Mixed-Valence Metal-Organic Framework Fe(1,2,3-Triazolate)$_2$$(BF_4)_x$. *J. Am. Chem. Soc.* **2018**, *140*, 8526−8534.

(15) Diamond, B. G.; Payne, L. I.; Hendon, C. H. Ligand Field Tuning of D-Orbital Energies in Metal-Organic Framework Clusters. *Commun. Chem.* **2023**, *6*, 67−73.

(16) Hmadeh, M.; Lu, Z.; Liu, Z.; Gándara, F.; Furukawa, H.; Wan, S.; Augustyn, V.; Chang, R.; Liao, L.; Zhou, F.; et al. New Porous Crystals of Extended Metal-Catecholates. *Chem. Mater.* **2012**, *24*, 3511−3513.

(17) Park, G.; Demuth, M. C.; Hendon, C. H.; Park, S. S. Acid-Dependent Charge Transport in a Solution-Processed 2D Conductive Metal-Organic Framework. *J. Am. Chem. Soc.* **2024**, *146*, 11493−11499.

(18) Apostol, P.; Gali, S. M.; Su, A.; Tie, D.; Zhang, Y.; Pal, S.; Lin, X.; Bakuru, V. R.; Rambabu, D.; Beljonne, D.; Dincă, M.; Vlad, A. Controlling Charge Transport in 2D Conductive MOFs−The Role of Nitrogen-Rich Ligands and Chemical Functionality. *J. Am. Chem. Soc.* **2023**, *145*, 24669−24677.

(19) Lu, Y.; Zhang, Y.; Yang, C. Y.; Revuelta, S.; Qi, H.; Huang, C.; Jin, W.; Li, Z.; Vega-Mayoral, V.; Liu, Y.; Huang, X.; Pohl, D.; Položij, M.; Zhou, S.; Cánovas, E.; Heine, T.; Fabiano, S.; Feng, X.; Dong, R. Precise tuning of interlayer electronic coupling in layered conductive metal-organic frameworks. *Nat. Commun.* **2022**, *13*, 7240.

(20) Debela, T. T.; Yang, M. C.; Hendon, C. H. Ligand-Mediated Hydrogenic Defects in Two-Dimensional Electrically Conductive Metal-Organic Frameworks. *J. Am. Chem. Soc.* **2023**, *145*, 11387−11391.

(21) Day, R. W.; Bediako, D. K.; Rezaee, M.; Parent, L. R.; Skorupskii, G.; Arguilla, M. Q.; Hendon, C. H.; Stassen, I.; Gianneschi, N. C.; Kim, P.; et al. Single Crystals of Electrically Conductive Two-Dimensional Metal-Organic Frameworks: Structural and Electrical Transport Properties. *ACS Cent. Sci.* **2019**, *5*, 1959−1964.

(22) Nam, K. W.; Park, S. S.; Dos Reis, R.; Dravid, V. P.; Kim, H.; Mirkin, C. A.; Stoddart, J. F. Conductive 2D Metal-Organic

Framework for High-Performance Cathodes in Aqueous Rechargeable Zinc Batteries. *Nat. Commun.* **2019**, *10*, 4948.
(23) Clough, A. J.; Skelton, J. M.; Downes, C. A.; de la Rosa, A. A.; Yoo, J. W.; Walsh, A.; Melot, B. C.; Marinescu, S. C. Metallic Conductivity in a Two-Dimensional Cobalt Dithiolene Metal-Organic Framework. *J. Am. Chem. Soc.* **2017**, *139*, 10863−10867.
(24) Sheberla, D.; Sun, L.; Blood-Forsythe, M. A.; Er, S.; Wade, C. R.; Brozek, C. K.; Aspuru-Guzik, A.; Dincă, M. High Electrical Conductivity in Ni_3(2,3,6,7,10,11-Hexaiminotriphenylene)$_2$, a Semiconducting Metal-Organic Graphene Analogue. *J. Am. Chem. Soc.* **2014**, *136*, 8859−8862.
(25) Skorupskii, G.; Trump, B. A.; Kasel, T. W.; Brown, C. M.; Hendon, C. H.; Dincă, M. Efficient and Tunable One-Dimensional Charge Transport in Layered Lanthanide Metal-Organic Frameworks. *Nat. Chem.* **2020**, *12*, 131−136.
(26) Skorupskii, G.; Dincă, M. Electrical Conductivity in a Porous, Cubic Rare-Earth Catecholate. *J. Am. Chem. Soc.* **2020**, *142*, 6920−6924.
(27) Nath, A.; Kumar, V.; Shukla, A.; Ghosh, H. N.; Mandal, S. Influence of Molecular Separation on through-Space Intervalence Transient Charge Transfer in Metal-Organic Frameworks with Cofacially Arranged Redox Pairs. *Angew. Chem., Int. Ed.* **2023**, *62*, No. e202308034.
(28) Brown, J. S. *CATNIP* (Version 1.9). [Software]. 2018. Available from https://github.com/JoshuaSBrown/QC_Tools.
(29) Kirkpatrick, J. An Approximate Method for Calculating Transfer Integrals Based on the Zindo Hamiltonian. *Int. J. Quantum Chem.* **2008**, *108*, 51−56.
(30) Bredas, J.-L.; Beljonne, D.; Coropceanu, V.; Cornil, J. Charge-Transfer and Energy-Transfer Processes in π-Conjugated Oligomersand Polymers: A Molecular Picture. *Chem. Rev.* **2004**, *104*, 4971−5004.
(31) Hsu, C.-P. The Electronic Couplings in Electron Transferand Excitation Energy Transfer. *Acc. Chem. Res.* **2009**, *42*, 509.
(32) Demuth, M. C.; Hendon, C. H. Linker Aromaticity Reduces Band Dispersion in 2D Conductive Metal-Organic Frameworks. *ACS Mater. Lett.* **2023**, *5*, 1476−1480.
(33) Sun, L.; Park, S. S.; Sheberla, D.; Dincă, M. Measuring and Reporting Electrical Conductivity in Metal-Organic Frameworks: Cd_2(TTFTB) as a Case Study. *J. Am. Chem. Soc.* **2016**, *138*, 14772−14782.
(34) Kresse, G.; Furthmüller, J. Efficiency of Ab-Initio Total Energy Calculations for Metals and Semiconductors Using a Plane-Wave Basis Set. *Comput. Mater. Sci.* **1996**, *6*, 15−50.
(35) Schimka, L.; Harl, J.; Kresse, G. Improved Hybrid Functional for Solids: The HSEsol Functional. *J. Chem. Phys.* **2011**, *134*, 024116.
(36) *Gaussian 09*, Revision A.02; 2016.

https://doi.org/10.1021/acsmaterialslett.4c01102
ACS Materials Lett. 2024, 6, 3909−3914